NASA Contractor Report 187486
ICASE Report No. 90–89

ICASE

ON THE RECEPTIVITY AND NON-PARALLEL STABILITY OF TRAVELLING DISTURBANCES IN ROTATING DISK FLOW

P. Balakumar
P. Hall
M. R. Malik

Contract No. NAS1–18605
December 1990

Institute for Computer Applications in Science and Engineering
NASA Langley Research Center
Hampton, Virginia 23665–5225

Operated by the Universities Space Research Association

NASA
National Aeronautics and
Space Administration

Langley Research Center
Hampton, Virginia 23665-5225

ON THE RECEPTIVITY AND NON-PARALLEL STABILITY OF TRAVELLING DISTURBANCES IN ROTATING DISK FLOW

P. Balakumar
High Technology Corporation
Hampton, VA 23666

P. Hall
University of Exeter
Exeter, UK

M. R. Malik
High Technology Corporation
Hampton, VA 23666

ABSTRACT

The generation and evolution of small amplitude long wavelength travelling disturbances in rotating disk flow is the subject of this paper. The steady rotational speed of the disk is perturbed so as to introduce high frequency oscillations in the flow field. Secondly, we introduce surface imperfections on the disk such as roughness elements. The interaction of these two disturbances will generate the instability waves whose evolution is governed by parabolic partial differential equations which are solved numerically. It is found that, for the class of disturbances considered here (wavelength on the order of Reynolds number), eigensolutions exist which decay or grow algebraically in the radial direction. However, these solutions grow only for frequencies larger than 4.58 times the steady rotational speed of the disk. The computed receptivity coefficient shows that there is an optimum size of roughness for which these modes are excited the most. The width of these roughness elements in the radial direction is about $.1r_0^*$ where r_0^* is the radial location of the roughness. It is also found that the receptivity coefficient is larger for a negative spanwise wavenumber than for a positive one. Typical wave angles found for these disturbances are about -26°.

This research was supported in part by the National Aeronautics and Space Administration under NASA Contract No. NAS1-18605 while the second author was in residence at the Institute for Computer Applications in Science and Engineering (ICASE), NASA Langley Research Center, Hampton, VA 23665. Additional support was provided SERC.

1. INTRODUCTION

In this paper, we investigate the receptivity and non-parallel stability problem for travelling disturbances in a rotating disk flow. A significant feature of the boundary-layer flow on the rotating disk is that its velocity component in the radial direction, the crossflow velocity, has an inflectional point. This causes an instability, often called crossflow instability, first noticed by Smith (1946) and investigated theoretically and experimentally by Gregory et al. (1955). When the crossflow component is combined in a particular direction with the velocity component in the azimuthal direction, they form a mean velocity profile which has an inflection point at which the velocity is zero. This permits an inviscid neutral disturbance with zero frequency which connects to unstable modes at other wavenumbers (see Stuart in Gregory, Stuart & Walker (1955)). The stationary disturbances appear as vortices, called crossflow vortices, which rotate in the same direction. This phenomena is also observed in other flow geometries such as rotating cones and swept wings, and it is this latter practical application which generates the interest in the problem since it is found that the crossflow instability dominates the boundary-layer transition process near the leading edge of a swept wing.

In the rotating disk flow, the crossflow vortices spiral outward at an angle whose magnitude is approximately 10°-14°, with respect to the azimuthal direction (Fig. 1), and these vortices first start to appear at a Reynolds number of about 286. Wilkinson and Malik (1983), using hot-wire techniques, mapped out the complete wave pattern on the disk and found that the stationary disturbances originate from isolated roughness sites on the disk. Mack (1985) computed the wave pattern observed in the Wilkinson-Malik experiment using the linearized stability equations and assuming a white spectrum at the source of the wave pattern. Malik (1986) calculated the neutral curve for stationary disturbances, and found numerically another stationary viscous mode which corresponded to zero wall-shear stress of the mean velocity profiles. At high Reynolds numbers on the lower branch of the neutral curve, the wavenumber α behaves like $\alpha = \text{const}/R^{1/2}$, and at the upper inviscid branch they behave like $\alpha \sim \text{const}$. Here α is the nondimensional wavenumber in the radial direction, which is nondimensionalized by the length scale $(\nu/\Omega_0)^{1/2}$, and R is the Reynolds number, defined by $R = r_e^*(\Omega_0/\nu)^{1/2}$, where ν is the kinematic viscosity, Ω_0 is the angular velocity of the disk, and r_e^* is the radius where the local stability analysis was done.

Hall (1986) developed an asymptotic analysis to investigate the two branches of the neutral curve. He showed that the inviscid mode is characterized by a two-layer structure. The upper deck is governed by the Rayleigh equation, and a thin layer near the wall is needed to satisfy the no-slip boundary condition at the wall. The lower branch neutral

curve is characterized by a triple-layer structure and has a long wave length. This mode has its structure fixed by a balance between viscous and Coriolis forces. At high Reynolds numbers, the lower branch neutral waves are inclined at about 39° to the radial direction. It is also observed that the formal asymptotic theory results, and the linear stability calculations based on parallel-flow assumption, agree for a large range of finite Reynolds number.

In a recent paper by Balakumar & Malik (1990) (referred to as BM below), linear stability characteristics of stationary and travelling disturbances in a rotating disk flow were presented. Figure (2) shows the neutral stability curves in the radial wavenumber α vs Reynolds number R plane for different nondimensional frequencies. Here the nondimensional frequency ω is defined as the ratio of the dimensional frequency of the disturbance ω^* to the rotational speed of the disk Ω_0. For a detailed discussion of this, the reader is referred to BM. In this paper, we are concerned with the lower branch neutral curve at high frequencies. It is seen from Fig. (2) that at high frequencies, ω = 6.0 and 7.9, the wavenumber α varies like R^{-1}. The waves for these modes are inclined at negative angles, see Fig. (1). For ω = 7.9, this angle is about -35.32°.

The stability results in BM have been obtained from linear stability theory with parallel flow assumptions being used. In the rotating disk case, this assumption amounts to locally replacing the variable radius r^* by the constant radius r_c^*. This approach is justified if the wavelength is much smaller than the radius r_c^*. This requirement is violated when the wavenumber is of the order of R^{-1}, and the validity of the Orr-Sommerfeld type approach becomes questionable. This is similar to the situation which exists in the Görtler problem, Hall (1982,1983). It was shown by Hall that, at 0(1) wavenumbers, the Görtler instability is governed by a parabolic type partial differential system. In this paper we investigate this R^{-1} BM mode of instability at high frequencies and allow for nonparallel effects in a self-consistent manner.

We formulate the problem as a receptivity problem similar to that analyzed for the Görtler case by Denier, Hall, & Seddougui (1990). We perturb the steady rotational speed of the disk so as to introduce high-frequency oscillations in the flow field. Secondly, we introduce imperfections on the surface as roughness elements. The interaction of these two flow effects, the unsteady one due to the oscillations of the disk and that introduced by the roughness, will generate the instability waves whose evolution is governed by parabolic partial differential equations. These partial differential equations are solved numerically. In Section 2 we describe the formulation of the receptivity problem for the rotating disk flow, the results are discussed in Section 3, and the conclusions are presented in Section 4.

2. FORMULATION OF THE PROBLEM

Consider an infinite disk rotating about its axis with angular velocity Ω_0 (Fig. (1)). We take cylindrical coordinates r^*, θ, z^* with $z^* = 0$ being the plane of the disk and assume that the fluid occupies the half space $z^* > 0$. Let $\overline{p}$, $\overline{u}$, $\overline{v}$, $\overline{w}$ denote the steady-state values of pressure and velocity in the r^*, θ, z^* directions, respectively, in the rotating coordinate frame. Von Karman's exact solution of the Navier-Stokes equations for steady laminar rotating-disk flow takes the form

$$\overline{u} = r^*\Omega_0 F(z) \ , \ \overline{v} = r^*\Omega_0 G(z) \ , \ \overline{w} = (\nu\Omega_0)^{1/2} H(z) \ , \ \overline{p} = \rho\nu\Omega_0 \pi(z) \tag{2.1}$$

where $z = z^*(\Omega_0 / \nu)^{1/2}$. The Navier-Stokes equations reduce to the following equations for F, G, H and P:

$$F^2 - (G+1)^2 + F'H - F'' = 0 \tag{2.2}$$

$$2F(G+1) + G'H - G'' = 0 \tag{2.3}$$

$$\pi' + HH' - H'' = 0 \tag{2.4}$$

$$2F + H' = 0 \tag{2.5}$$

where the prime denotes differentiation with respect to z. The boundary conditions are:

$$F = 0, \ G = 0, \ H = 0 \qquad (z = 0) \tag{2.6}$$

$$F = 0 \quad G = -1 \qquad (z \to \infty) \tag{2.7}$$

In the following analysis the variables are nondimensionalized by:

velocity - $r_e^*\Omega_0$,

length - $\left(\frac{\nu}{\Omega_0}\right)^{1/2}$,

pressure - $\rho r_e^{*2}\Omega_0^2$,

time - $\left(\frac{\nu}{\Omega_0}\right)^{1/2} \frac{1}{r_e^*\Omega_0}$.

The Reynolds number is defined by

$$R = r_e^*\left(\frac{\Omega_0}{\nu}\right)^{1/2} \ , \tag{2.8}$$

where r_c^* is a typical radial length scale.

Let us write the instantaneous nondimensional velocities u, v, w and pressure p as

$$u(r,\theta,z,t) = \frac{r}{R}F(z) + U(r,\theta,z,t) \quad , \tag{2.9}$$

$$v(r,\theta,z,t) = \frac{r}{R}G(z) + V(r,\theta,z,t) \quad , \tag{2.10}$$

$$w(r,\theta,z,t) = \frac{1}{R}H(z) + W(r,\theta,z,t) \quad , \tag{2.11}$$

$$p(r,\theta,z,t) = \frac{1}{R^2}\pi(z) + P(r,\theta,z,t) \quad , \tag{2.12}$$

where U, V, W are nondimensional perturbations from the steady mean flow. We substitute these expressions into the Navier-Stokes equations in the rotating frame and obtain the following nonlinear perturbation equations for U, V, W, and P.

$$\frac{\partial U}{\partial t} + \frac{r}{R}F\frac{\partial U}{\partial r} + \frac{G}{R}\frac{\partial U}{\partial \theta} + \frac{H}{R}\frac{\partial U}{\partial z} + \frac{F}{R}U + \frac{r}{R}WF' - \frac{2}{R}(G+1)V - \frac{V^2}{r} + U\frac{\partial U}{\partial r} + \frac{V}{r}\frac{\partial U}{\partial \theta} + W\frac{\partial U}{\partial z}$$

$$= -\frac{\partial P}{\partial r} + \frac{1}{R}\left\{\frac{\partial^2 U}{\partial r^2} + \frac{1}{r^2}\frac{\partial^2 U}{\partial \theta^2} + \frac{1}{r}\frac{\partial U}{\partial r} + \frac{\partial^2 U}{\partial z^2} - \frac{U}{r^2} - \frac{2}{r^2}\frac{\partial V}{\partial \theta}\right\} \quad , \tag{2.13}$$

$$\frac{\partial V}{\partial t} + \frac{r}{R}F\frac{\partial V}{\partial r} + \frac{G}{R}\frac{\partial V}{\partial \theta} + \frac{H}{R}\frac{\partial V}{\partial z} + \frac{F}{R}V + \frac{r}{R}WG' + \frac{2}{R}(G+1)U + \frac{UV}{r} + U\frac{\partial V}{\partial r} + \frac{V}{r}\frac{\partial V}{\partial \theta} + W\frac{\partial V}{\partial z}$$

$$= -\frac{1}{r}\frac{\partial P}{\partial \theta} + \frac{1}{R}\left\{\frac{\partial^2 V}{\partial r^2} + \frac{1}{r^2}\frac{\partial^2 V}{\partial \theta^2} + \frac{1}{r}\frac{\partial V}{\partial r} + \frac{\partial^2 V}{\partial z^2} - \frac{V}{r^2} + \frac{2}{r^2}\frac{\partial U}{\partial \theta}\right\} \quad , \tag{2.14}$$

$$\frac{\partial W}{\partial t} + \frac{r}{R}F\frac{\partial W}{\partial r} + \frac{G}{R}\frac{\partial W}{\partial \theta} + \frac{H}{R}\frac{\partial W}{\partial z} + \frac{1}{R}WH' + U\frac{\partial W}{\partial r} + \frac{V}{r}\frac{\partial W}{\partial \theta} + W\frac{\partial W}{\partial z}$$

$$= -\frac{\partial P}{\partial z} + \frac{1}{R}\left\{\frac{\partial^2 W}{\partial r^2} + \frac{1}{r^2}\frac{\partial^2 W}{\partial \theta^2} + \frac{1}{r}\frac{\partial W}{\partial r} + \frac{\partial^2 W}{\partial z^2}\right\} \quad , \tag{2.15}$$

$$\frac{U}{r} + \frac{\partial U}{\partial r} + \frac{1}{r}\frac{\partial V}{\partial \theta} + \frac{\partial W}{\partial z} = 0. \tag{2.16}$$

Here r is the nondimensional radius and t is the nondimensional time. We must solve (2.13) - (2.16) subject to the no-slip condition at the wall, whereas sufficiently far away from the wall we insist that the disturbances vanish. We are going to investigate the high frequency lower-branch instability mode for which the wavenumber varies like R^{-1} at high Reynolds numbers as discussed in BM.

We introduce a disturbance into the steady motion first by perturbing the speed of rotation of the disk to

$$\Omega = \Omega_0\left(1+\Delta e^{-i\omega^* t^*}\right) \quad , \tag{2.17}$$

and second by introducing a hump on the surface of the disk (Fig. 1). Here ω^* is the dimensional frequency of the oscillations which may, for example, simulate an acoustic disturbance. The shape of the hump is defined by

$$z^* = \left(\frac{\nu}{\Omega_0}\right)^{1/2} \delta\, f\left(\frac{r^*}{r_e^*}, \theta\right) \quad , \tag{2.18}$$

where f is a function of (r^* / r_e^*) and θ; δ and Δ are small scalar parameters with $\delta, \Delta << 1$. In nondimensional form (2.17) and (2.18) become

$$\Omega = \Omega_0\left(1+\Delta\, e^{-i\omega/Rt}\right) \quad , \tag{2.19}$$

and

$$z = \delta\, f\left(\frac{r}{R}, \theta\right) \quad , \tag{2.20}$$

where ω is the nondimensional frequency defined by $\omega = \omega^* / \Omega_0$. Since we are seeking solutions which are linear in δ, we can look for Fourier series solutions in the θ direction. We expand $f(r/R, \theta)$ in Fourier series as

$$f\left(\frac{r}{R}, \theta\right) = \sum_{\beta=-\infty}^{\infty} \bar{f}\left(\frac{r}{R}, \beta\right) e^{i\beta\theta} \quad . \tag{2.22}$$

This will permit us to perform the analysis in the Fourier space β. We will assume that Reynolds number R is large and seek solutions which are linear in δ and Δ. The perturbations U, V, W and P are written as

$$\begin{aligned} U = \Delta \frac{r}{R}\tilde{F}(z)e^{-i\omega/Rt} \quad & + \delta \frac{r}{R}\bar{F}\left(\frac{r}{R}, z\right)e^{i\beta\theta} \\ & + \Delta\cdot\delta\,\hat{u}\left(\frac{r}{R}, z\right)e^{-i\omega/Rt}e^{i\beta\theta} \\ & + \text{higher order terms} \quad , \end{aligned} \tag{2.23}$$

$$\begin{aligned} V = \Delta \frac{r}{R}\tilde{G}(z)e^{-i\omega/Rt} \quad & + \delta \frac{r}{R}\bar{G}\left(\frac{r}{R}, z\right)e^{i\beta\theta} \\ & + \Delta\cdot\delta\,\hat{v}\left(\frac{r}{R}, z\right)e^{-i\omega/Rt}e^{i\beta\theta} \\ & + \text{higher order terms} \quad , \end{aligned} \tag{2.24}$$

$$W = \Delta \frac{r}{R}\tilde{H}(z)e^{-i\omega/Rt} \quad +\delta\frac{1}{R}\overline{H}\left(\frac{r}{R},z\right)e^{i\beta\theta}$$
$$+\Delta\cdot\delta\frac{1}{R}\hat{w}\left(\frac{r}{R},z\right)e^{-i\omega/Rt}e^{i\beta\theta}$$
$$+\text{higher order terms} \quad , \tag{2.25}$$

$$P = \Delta \frac{1}{R^2}\tilde{P}(z)e^{-i\omega/Rt} \quad +\delta\frac{1}{R^2}\overline{P}\left(\frac{r}{R},z\right)e^{i\beta\theta}$$
$$+\Delta\cdot\delta\frac{1}{R^2}\hat{p}\left(\frac{r}{R},z\right)e^{-i\omega R/t}e^{i\beta\theta} \quad . \tag{2.26}$$

We identify $(\tilde{F},\tilde{G},\tilde{H},\tilde{P})$ as the flowfield induced by the oscillations of the disk, $(\overline{F},\overline{G},\overline{H},\overline{P})$ as the flowfield induced by the hump, and $(\hat{u},\hat{v},\hat{w},\hat{p})$ as the flowfield produced by the interaction between the first two flow fields. Let us assume that the factor $\overline{r} = r/R$ is 0(1). Substituting the above expressions (2.23) - (2.26) into the equations (2.13) - (2.16) and collecting terms of the same order we obtain a sequence of equations for the induced fields. At order Δ, we obtain

$$(-i\omega + 2F)\tilde{F} + H\tilde{F}' - 2(G+1)\tilde{G} + F'\tilde{H} - \tilde{F}'' = 0 \tag{2.27}$$

$$(-i\omega + 2F)\tilde{G} + H\tilde{G}' + 2(G+1)\tilde{F} + G'\tilde{H} - \tilde{G}'' = 0 \tag{2.28}$$

$$(-i\omega + H')\tilde{H} + H\tilde{H}' + \tilde{P} - \tilde{H}'' = 0 \tag{2.29}$$

$$2\tilde{F} + \tilde{H}' = 0. \tag{2.30}$$

The boundary conditions at the solid boundary are

$$\tilde{F}(0) = \tilde{H}(0) = 0 \tag{2.31}$$

$$\tilde{G}(0) = 1 \ . \tag{2.32}$$

Far away from the surface of the disk the disturbance should decay exponentially. This gives

$$\tilde{F}' - \mu\tilde{F} = 0 \tag{2.33}$$

$$\tilde{G}' - \mu\tilde{G} = 0 \tag{2.34}$$

where

$$\mu = \frac{H(\infty) - \sqrt{H^2(\infty) - 4i\omega}}{2} \tag{2.35}$$

and the real part of μ is less than zero. For order δ we obtain the following equations for $\overline{F},\overline{G},\overline{H}$ and $\overline{P}$:

$$(2F+i\beta G)\overline{F}+\bar{r}F\frac{\partial\overline{F}}{\partial\bar{r}}+H\frac{\partial\overline{F}}{\partial z}-2(G+1)\overline{G}+F'\overline{H}=\frac{\partial^2\overline{F}}{\partial z^2} \quad , \tag{2.36}$$

$$(2F+i\beta G)\overline{G}+\bar{r}F\frac{\partial\overline{G}}{\partial\bar{r}}+H\frac{\partial\overline{G}}{\partial z}+2(G+1)\overline{F}+G'\overline{H}=\frac{\partial^2\overline{G}}{\partial z^2} \quad , \tag{2.37}$$

$$\bar{r}F\frac{\partial\overline{H}}{\partial\bar{r}}+i\beta G\overline{H}+H\frac{\partial\overline{H}}{\partial z}+H'\overline{H}=-\frac{\partial\overline{P}}{\partial z}+\frac{\partial^2\overline{H}}{\partial z^2} \quad , \tag{2.38}$$

$$2\overline{F}+\bar{r}\frac{\partial F}{\partial\bar{r}}+i\beta\overline{G}+\frac{\partial\overline{H}}{\partial z}=0 \quad . \tag{2.39}$$

The appropriate boundary conditions are

$$\overline{F}(0)=-F'(0)\tilde{f}(\bar{r},\beta) \tag{2.40}$$

$$\overline{G}(0)=-G'(0)\tilde{f}(\bar{r},\beta) \tag{2.41}$$

$$\overline{H}(0)=0 \tag{2.42}$$

The solution of Eq. (2.36-2.42) is:

$$\overline{F}(z)=-F'(z)\tilde{f}(\bar{r},\beta) \quad , \tag{2.43}$$

$$\overline{G}(z)=-G'(z)\tilde{f}(\bar{r},\beta) \quad , \tag{2.44}$$

$$\overline{H}(z)=\left\{2\tilde{f}(\bar{r},\beta)+\bar{r}\frac{\partial\tilde{f}}{\partial\bar{r}}\right\}F(z)+i\beta G(z)\tilde{f}(r,\beta) \quad , \tag{2.45}$$

and $\overline{P}(z)$ can be obtained from Eq. (2.38). At order $\Delta\delta$, we obtain the equations for the induced disturbances $\hat{u},\hat{v},\hat{w}$ and $\hat{p}$:

$$\frac{\partial^2\hat{u}}{\partial z^2}-(-i\omega+i\beta G+F)\hat{u}-\bar{r}F\frac{\partial\hat{u}}{\partial\bar{r}}-H\frac{\partial\hat{u}}{\partial z}-\bar{r}\hat{w}F'+2(G+1)\hat{v}=\left\{-2\bar{r}\tilde{G}\overline{G}+\bar{r}\tilde{F}\left(\overline{F}+\bar{r}\frac{\partial\overline{F}}{\partial\bar{r}}\right)\right.$$

$$\left.+\bar{r}\overline{F}F+i\beta\tilde{G}\overline{F}\bar{r}+\bar{r}\tilde{H}\frac{\partial\overline{F}}{\partial z}+\bar{r}\overline{H}\frac{\partial\tilde{F}}{\partial z}\right\} \quad , \tag{2.46}$$

$$\frac{\partial^2\hat{v}}{\partial z^2}-(-i\omega+i\beta G+F)\hat{v}-\bar{r}F\frac{\partial\hat{v}}{\partial\bar{r}}-H\frac{\partial\hat{v}}{\partial z}-\bar{r}G'\hat{w}-2(G+1)\hat{u}=\bar{r}\left(\tilde{F}\overline{G}+\overline{F}\tilde{G}\right)+\bar{r}\tilde{F}\left(\overline{G}+\bar{r}\frac{\partial\overline{G}}{\partial\bar{r}}\right)$$

$$+\bar{r}\bar{F}\tilde{G}+i\beta\tilde{G}\bar{G}\bar{r}+\bar{r}\tilde{H}\frac{\partial\bar{G}}{\partial z}+\bar{r}\bar{H}\frac{\partial\tilde{G}}{\partial z} \quad , \tag{2.47}$$

$$-\frac{\partial\hat{p}}{\partial z}=-\frac{\partial^2\hat{w}}{\partial z^2}+(-i\omega+i\beta G+H')\hat{w}+\bar{r}F\frac{\partial\hat{w}}{\partial\bar{r}}+H\frac{\partial\hat{w}}{\partial z}+\bar{r}\tilde{F}\frac{\partial\bar{H}}{\partial\bar{r}}+i\beta\tilde{G}\bar{G}+\tilde{H}\frac{\partial\bar{H}}{\partial z}+\bar{H}\frac{\partial\tilde{H}}{\partial z} \quad , \tag{2.48}$$

$$\hat{u}+\bar{r}\frac{\partial\hat{u}}{\partial\bar{r}}+i\beta\hat{v}+\bar{r}\frac{\partial\hat{w}}{\partial z}=0 \quad . \tag{2.49}$$

The appropriate boundary conditions are

$$\hat{u}(0)=-\tilde{F}'(0)\bar{r}\bar{f}(\bar{r},\beta) \quad , \tag{2.50}$$

$$\hat{v}(0)=-\tilde{G}'(0)\bar{r}\bar{f}(\bar{r},\beta) \quad , \tag{2.51}$$

$$\hat{w}(0)=0 \quad . \tag{2.52}$$

It is easy to verify that if we write

$$\hat{u}=-\tilde{F}'(z)\bar{r}\bar{f}(\bar{r},\beta)+u_1 \quad , \tag{2.53}$$

$$\hat{v}=-\tilde{G}'(z)\bar{r}\bar{f}(\bar{r},\beta)+v_1 \quad , \tag{2.54}$$

$$\hat{w}=\left\{2\bar{f}+\bar{r}\frac{\partial\bar{f}}{\partial\bar{r}}\right\}\tilde{F}(z)+i\beta\tilde{G}\bar{f}+w_1 \quad , \tag{2.55}$$

then Eq. (2.46), (2.47) and (2.49) take the form

$$\frac{\partial^2u_1}{\partial z^2}=(-i\omega+i\beta G+F)u_1+\bar{r}F\frac{\partial u_1}{\partial\bar{r}}+H\frac{\partial u_1}{\partial z}+\bar{r}F'w_1-2(G+1)v_1 \quad , \tag{2.56}$$

$$\frac{\partial^2v_1}{\partial z^2}=(-i\omega+i\beta G+F)v_1+\bar{r}F\frac{\partial v_1}{\partial\bar{r}}+H\frac{\partial v_1}{\partial z}+\bar{r}G'w_1+2(G+1)u_1 \quad , \tag{2.57}$$

$$\bar{r}\frac{\partial w_1}{\partial z}+u_1+\bar{r}\frac{\partial u_1}{\partial\bar{r}}+i\beta v_1=0 \quad , \tag{2.58}$$

with the boundary conditions

$$u_1(\bar{r},0)=0 \quad , \tag{2.59}$$

$$v_1(\bar{r},0)=0 \quad , \tag{2.60}$$

$$w_1(\bar{r},0)=-i\beta\bar{f}(\bar{r},\beta) \quad . \tag{2.61}$$

The boundary conditions at the far field are

$$u_1'-\tilde{\mu}u_1=0 \tag{2.62}$$

$$v_1' - \tilde{\mu} w_1 = 0 \tag{2.63}$$

where

$$\tilde{\mu} = \frac{H(\infty) - \sqrt{H(\infty)^2 - i(\omega + \beta)}}{2} \tag{2.64}$$

and the real part of $\tilde{\mu}$ is less than zero. Equation (2.48) can be integrated to solve for pressure $\hat{p}$. We observe that the above system of equations is of the parabolic type. The inhomogenity appears as the normal boundary condition $w_1(\bar{r},0) = -i\beta\bar{f}(\bar{r},\beta)$. Therefore, if we specify ω, β and $\bar{f}(\bar{r},\beta)$ we can integrate these equations marching in $\bar{r}$. The equations were solved using the two-point fourth-order compact scheme in the z direction and second-order upwind scheme in $\bar{r}$ direction (Spall & Malik (1989)).

We note that the system (2.56-2.58) permits eigensolutions of the form

$$\begin{Bmatrix} u_1 \\ v_1 \\ w_1 \end{Bmatrix} = r^{\gamma} \begin{Bmatrix} u_0(z) \\ v_0(z) \\ \dfrac{w_0(z)}{r} \end{Bmatrix} , \tag{2.65}$$

where γ is a complex number and (u_0, v_0, w_0) satisfy,

$$\frac{d^2 u_0}{dz^2} = (-i\omega + i\beta G + F)u_0 + \gamma F u_0 + H\frac{du_0}{dz} + w_0 F' - 2(G+1)v_0 \quad , \tag{2.66}$$

$$\frac{d^2 v_0}{dz^2} = (-i\omega + i\beta G + F)v_0 + \gamma F v_0 + H\frac{dv_0}{dz} + w_0 G' + 2(G+1)u_0 \quad , \tag{2.67}$$

$$\frac{dw_0}{dz} + u_0 + \gamma u_0 + i\beta v_0 = 0 \quad , \tag{2.68}$$

with the boundary conditions $u_0(0) = v_0(0) = w_0(0) = 0$ and u, v and w decay at infinity. Therefore, γ is the eigenvalue of the system and determines whether the disturbance grows or decays algebraically in the radial direction. If in the parallel flow linearized stability equations (2.16-2.19) of BM, we replace $\alpha = \alpha_0 / R$, $\beta = \beta_0 / R$, $\bar{\omega} = \omega / R$ and neglect all the $1/R^2$ terms, we obtain the same equations as above (2.66-2.68) with $i\alpha$ replaced by γ. Therefore, the solutions obtained for the high frequency ($1/R$) mode in the earlier paper are to be interpreted as algebraic and not as exponentially growing/decaying solutions. In fact, the linearized Navier-Stokes equations in a rotating coordinate system (equations (2.11-2.14) in BM) have solutions of the form

$$\tilde{u} = r^{\gamma}\left\{\tilde{\tilde{u}}_0(z) + \frac{\tilde{\tilde{u}}_1(z)}{r^2} + \cdots + \frac{\tilde{\tilde{u}}_n(z)}{r^{2n}} + \cdots\right\} \quad ,$$

$$\tilde{v} = r^{\gamma}\left\{\tilde{\tilde{v}}_0(z) + \frac{\tilde{\tilde{v}}_1(z)}{r^2} + \cdots + \frac{\tilde{\tilde{v}}_n(z)}{r^{2n}} + \cdots\right\} \quad ,$$

$$\tilde{w} = r^{\gamma}\left\{\frac{\tilde{\tilde{w}}_0(z)}{r} + \frac{\tilde{\tilde{w}}_1(z)}{r^2} + \cdots + \frac{\tilde{\tilde{w}}_n(z)}{r^{2n+1}} + \cdots\right\} \quad ,$$

$$\tilde{p} = \frac{r^{\gamma}}{R}\left\{\frac{\tilde{\tilde{p}}_0(z)}{r} + \frac{\tilde{\tilde{p}}_1(z)}{r^2} + \cdots + \frac{\tilde{\tilde{p}}_n(z)}{r^{2n+1}} + \cdots\right\} \quad .$$

This solution exists for all the frequencies ω and all azimuthal wavenumbers β. However, we will see in the next section that the real part of γ is positive only for frequencies $\omega > 4.58$ and for a certain range of β values, and thus the algebraic instability is not present for lower frequencies.

3. RESULTS

First we will present the values of γ obtained from the eigenvalue system (2.66-2.68). The results are depicted in Table 1.

Table 1

ω	β	γ
+4.0	+0.0	(-.50388,15.318)
	-1.0	(-.48892,13.176)
	-2.0	(-.49032,10.829)
	-3.0	(-.54533,8.089)
+4.6	-2.0	(-.03848,13.484)
	-1.0	(-.00918,15.783)
	0.0	(.00422,17.916)
	1.0	(.00921,19.936)
	2.0	(.00753,21.874)
	3.0	(.00186,23.748)
	4.0	(-.00675,25.570)
+7.9	-8.0	(-1.3621,9.593)
	-7.0	(1.1622,14.652)
	-6.0	(1.6793,18.261)
	-5.0	(1.9842,21.249)
	-4.0	(2.2082,23.919)
	-2.0	(2.5397,28.716)
	0.0	(2.7884,33.074)
	2.0	(2.9893,37.156)
	4.0	(3.1582,41.045)

We observe that the real part of γ is positive for frequencies larger than 4.58, however, this occurs only for a certain range of β values. For $\omega = 4.6$, real (γ) is positive in the range of β = 0.0 to 3.0 and for $\omega = 7.9$, this range is from -7.0 to 40. These results are in agreement with the BM results reproduced in Figure 2 which shows that 1/*R* mode instability is present only for frequencies higher than 4.58. The unstable modes computed by BM for frequencies lower than 4.58 do not belong to this class of instability.

Now we present the results for the receptivity coefficient associated with the 1/*R* mode discussed above. First we consider the case where $\bar{f}(\bar{r},\beta)$ takes the form

$$\bar{f}(\bar{r},\beta) = e^{-x^2} \quad ,$$

with

$$x = \sqrt{\sigma}(\bar{r} - \bar{r}_0) \quad .$$

Here $\bar{r}_0$ is the location of the hump and will be taken as $\bar{r}_0 = 1$, which is equivalent to defining the r_e^* based on the radial location of the hump. The parameter σ determines the spread of the hump in the radial direction.

Figures 3, 4 and 5 show the downstream development of the amplitude of u_1, v_1 and w_1 (Eqs. (2.56-2.58)) for the case $\omega = 7.9$, $\beta = -7$ and $\sigma = 40.0$. In these figures, the vertical axis shows the normal coordinate z and the different curves are plotted at different $\bar{r}$ = .6, .7, .8, .9, 1.0, 1.1, 1.25, 1.3, 1.4, 1.6 and 1.9. We notice that the initial form of the radial disturbance velocity component u_1 shows two maxima, and the lower maximum disappears while the amplitude of the upper maximum increases continuously with $\bar{r}$. The distribution of the amplitude of the normal velocity component w_1 shows that at the edge of the boundary layer it approaches a constant value which increases with increasing $\bar{r}$.

In Figs. 6, 7, 8, and 9 we plot the maximum amplitude of the velocity components u_1, v_1, and w_1 against the coordinate x for various values of σ with $\beta = -7$ and $\omega = 7.9$. For u_1 we take the maximum amplitude at the outer maximum point and for w_1 we take the maximum amplitude as the amplitude at the edge of the boundary layer. We observe two different types of curves for a fixed σ. For an x less than about .5, the amplitude pattern appears to be Gaussian shaped, and beyond that, the amplitude increases with increasing x. We identify that the first part is due to the direct influence of the wall and the second growing part is due to the instability. Figure 9 is the same as Fig. 7 and the curve $A = C_1(\beta,\sigma,\omega)\bar{r}^{\gamma}$ is plotted for σ = 10, 20, 100, and 200. Here γ is the eigenvalue obtained from Eq. (2.66-2.68) for $\omega = 7.9$ and $\beta = -7$ and is equal to (1.1622, 14.652). $C_1(\beta,\sigma,\omega)$ is a measure of the receptivity coefficient of these modes to the excitation we considered in this paper. From Fig. 9 it is clear that there exists downstream an algebraic instability of the form r^{γ} and there are no

other eigenfunctions which exist for the system (2.56-2.58). The receptivity coefficient $C_1(\beta,\sigma,\omega)$ is given in Table 2 for $\omega = 7.9$ and $\beta = -7$ for different σ values.

Table 2

σ	$C_1(\beta = -7, \sigma, \omega = 7.9)$	$\lvert C_1 \rvert$
5	(.00135,.00324)	.00352
10	(-.00391,.00983)	.01058
20	(-.04381,.01251)	.04556
40	(-.11258,.01124)	.11314
100	(-.16154,.02733)	.16384
200	(-.14827,.03586)	.15254
1000	(-.08145,.02089)	.08409
2000	(-.05812,.01693)	.06054

The receptivity coefficient increases with σ up to $\sigma = 100$ and then decreases. Therefore, we conclude that there exists an optimum size for which instabilities are excited the most. In Fig. 10, we plot the maximum amplitude of v_1 for $\omega = 7.9$, $\sigma = 100$ for different β values. The figure shows that the waves are excited for the range of β values $\beta = -7$ to $\beta = 20$. The receptivity coefficients are larger for negative β values than for positive β values.

Next, we will present the cumulative wave pattern produced downstream of the roughness site. We will consider the case $\omega = 7.9$ and $\sigma = 100$ and the roughness element defined by

$$f(r,\theta) = e^{-x^2} S(\theta) \quad ,$$

where

$$x = \sqrt{\sigma}(\bar{r} - 1.0) \quad ,$$

and $S(\theta)$ defines the shape in the azimuthal direction. We consider the triangular shape defined by

$$S(\theta) = \frac{1}{a}(\theta + a) \quad ; \quad -a \le \theta \le 0$$

$$= \frac{1}{b}(b - \theta) \quad ; \quad 0 \le \theta \le b$$

where a, b are positive numbers which are in the range $0 \le a, b \le \pi$. If a equals b we get the symmetric shape; otherwise, we get the asymmetric case. We will present the results for the cases $a = b = .05$. The Fourier transform of $S(\theta)$ is

$$S(\theta) = \sum_{-\infty}^{\infty} \bar{S}(\beta) e^{i\beta\theta}$$

where

$$\bar{S}(\beta) = \frac{1}{2\pi}(a+b) \quad ; \quad \beta = 0$$

$$\bar{S}(\beta) = \frac{1}{2\pi}\frac{1}{\beta^2}\left\{\frac{1-e^{i\beta a}}{a} + \frac{1-e^{-i\beta b}}{b}\right\} \quad ; \quad \beta \neq 0 \quad .$$

Figure 11 shows the contour plot in $(\bar{r}, \theta)$ plane of the real part of $v_1(\bar{r}, \theta, z, t)$ at the height z = 1.5 for the case ω = 7.9 and σ = 100, a = .05 and b = .05. The roughness element is located at $\bar{r}_o$ = 1 and is denoted by the point x. Near the roughness we see the effect of the roughness, and downstream of the roughness we observe the instability waves emerging from the wake. Contours of zero amplitude are highlighted by thick lines. These waves are inclined at angles of about -26°. The wavelength in the radial direction is about 1.0 and the number of waves in the azimuthal direction β is about 6.

In Fig. 12 we plot the maximum amplitude of $|V_1|$ for ω = 4.6 for different β and σ values. We see that there is only weak instability for this frequency for certain values of β. Figures 13 and 14 show the results for frequencies ω = 4.0 and 0.0. For these frequencies, all the disturbances decay downstream. All these conclusions agree with our previous calculations for γ and the results of BM that the $1/R$ instability is present only for $\omega > 4.58$.

4. CONCLUDING REMARKS

The receptivity and non-parallel stability of travelling disturbances of long wavelength (on the order of Reynolds number R) are investigated. The non-parallel effects are included in a self-consistent manner. It is shown that eigensolutions exist which grow or decay algebraically in the radial direction. It is established that the solutions obtained for the high frequency ($1/R$) mode in the earlier paper of BM are to be interpreted as algebraic and not as exponentially growing/decaying solutions. These algebraic-type solutions exist for all frequencies ω and all spanwise wavenumbers β. However, growing disturbances exist only for frequencies larger than 4.58 times the disk rotational frequency and for a certain range of β values which is in agreement with the results of BM.

The receptivity calculations show that there exists an optimum size of roughness for which instabilities are excited the most. For example, the receptivity coefficient C_1 for frequency ω = 7.9 with spanwise wavenumber β = -7 is .01, .16 and .084 when σ = 10, 100 and 1000, respectively. Gaussian shaped roughness elements with σ = 100 correspond to a

roughness element with a spread of about $.1r_0^*$ in the radial direction, where r_0^* is the location of the roughness. This shows that very narrow or broad roughness elements will not excite these modes efficiently. It is also observed that the receptivity coefficients are larger for negative β values than for positive β values. Hence, if these modes are excited they will align along negative angles.

The cumulative wave pattern produced from an isolated roughness element shows that the waves are inclined at about -26° and the wavelength in the radial direction is about 1.0. In dimensional variables, the wavelength 1.0 equals to r_0^* where the r_0^* is the location of the element. In some experiments performed by Faller and Kaylor (1966), in Ekman layer and rotating disk boundary layer, the waves oriented at negative angles have been observed at finite Reynolds numbers. These waves were rapidly moving and had long wavelengths compared to cross-flow vortices. Even though there seems to be some similarities between these computed algebraic modes and the experimental observations, more measurements have to be done to draw any definite conclusions.

Another remaining question is how the lower branch exponential-type solutions join with this algebraic mode. For example, consider the neutral stability curve for frequency $\omega = 6.0$ shown in Fig. 2. The lower branch neutral curve, which is asymptote to the neutral curve for stationary disturbances, is an exponential-type solution. We see that this curve turns around at a Reynolds number of 3×10^6 and becomes a $1/R$ mode. However, we discussed that this $1/R$ mode is actually an algebraic-type mode. Therefore, why does the lower branch neutral curve, which is asymptote to the neutral curve for stationary disturbances, turn around, and what is its subsequent behavior, are the remaining questions.

ACKNOWLEDGEMENTS

This work was sponsored by NASA Langley Research Center under Contracts NAS1-18240 (PB & MRM) and NAS1-18605 (PH).

REFERENCES

Balakumar, P.; and Malik, M. R.: to appear in *Theoretical & Compu. Fluid Dyn*, 1990.

Denier, J. P.; Hall P.; and Seddougui S.: ICASE Report No. 90-31, 1990 .

Faller, A. J.; and Kaylor. R. E.: in *Dynamics of Fluids and Plasmas*, Academic Press 309, Edited by S. I. Pai et al, 1966.

Gregory, N.; Stuart, J. T.; and Walker, W. S.: *Proc. Trans. Roy. Soc. Lond. A* **248** pp. 155, 1955

Hall, P.: *J. Fluid Mech.* **124** pp. 475, 1982.

Hall, P.: *J. Fluid Mech.* **130** pp. 41, 1983.

Hall, P.: *Proc. R. Soc. Lond. A* **406** pp. 93, 1986.

Mack, L. M.: AIAA Paper 86-0490, 1985.

Malik, M. R.: *J. Fluid Mech.* **164** pp. 275, 1986.

Smith, N. H.: NACA Tech. Note 1227, 1946.

Spall, R. E.; and Malik, M. R.: *Physics of Fluids A1* **11**, 1989.

Wilkinson, S. P.; and Malik M. R.: AIAA Paper 83-1760, 1983. (Also, 1985 *AIAA J.* **23** pp. 588.)

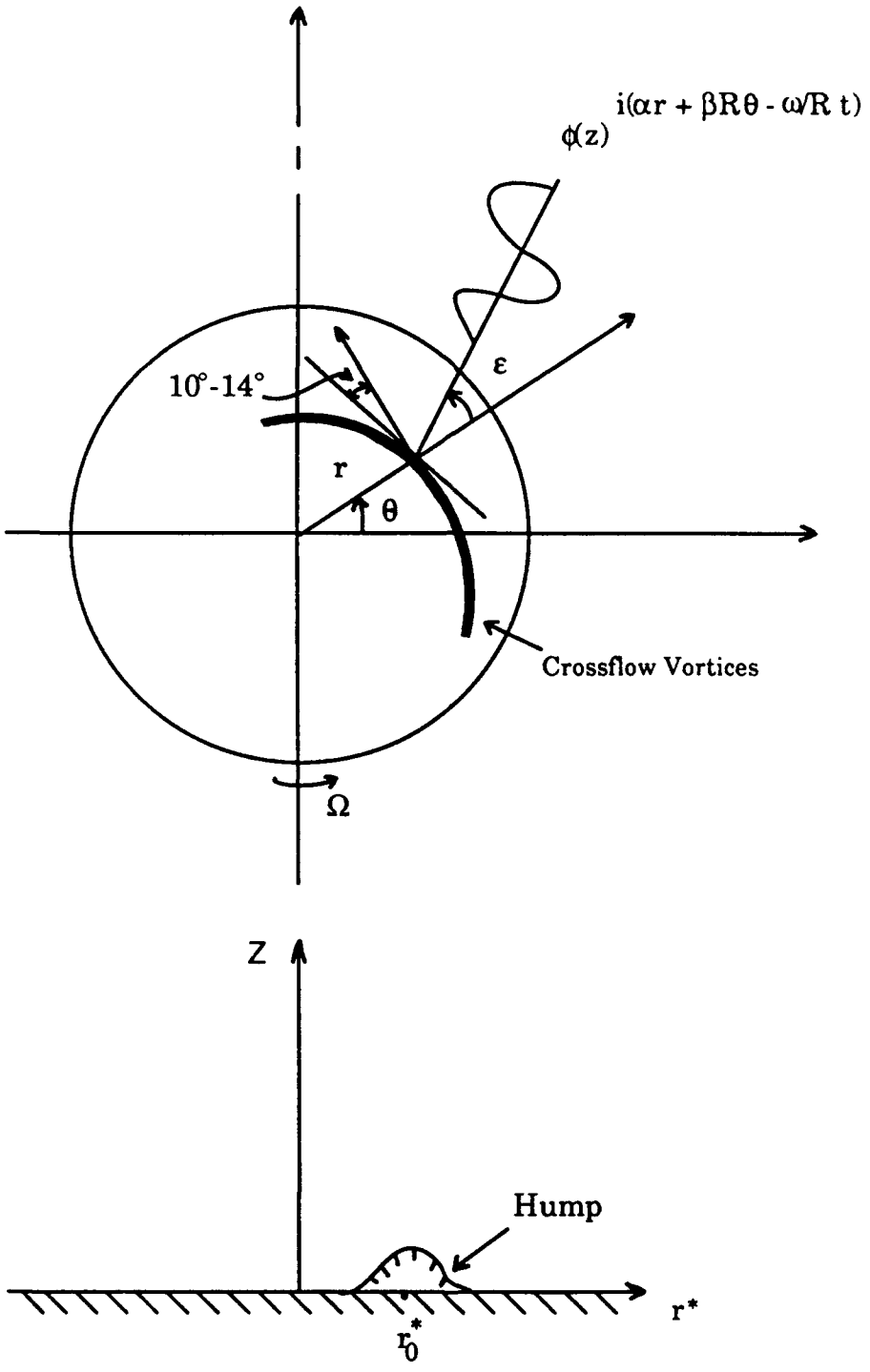

Fig. 1. Schematic of rotating-disk flow.

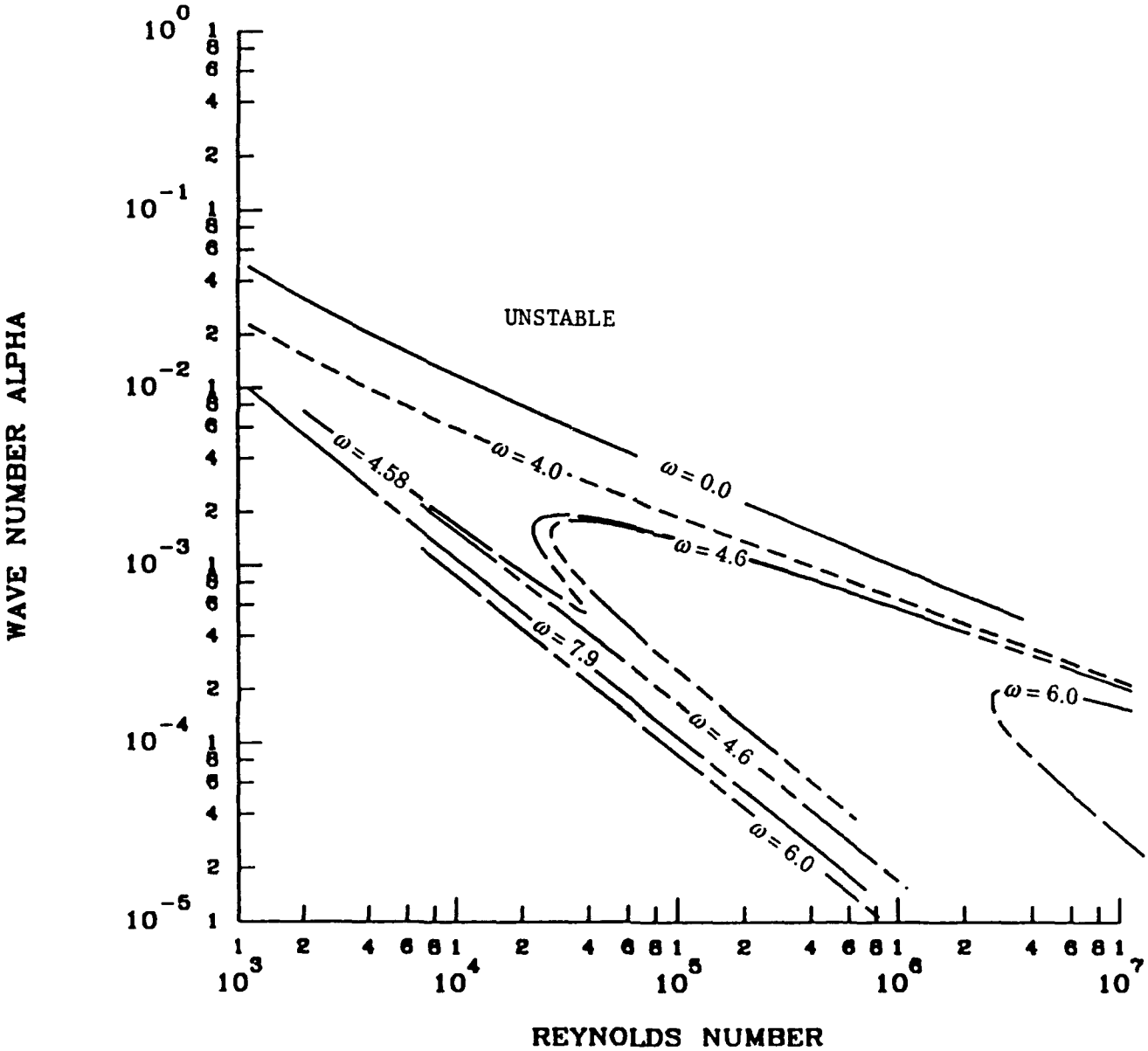

Fig. 2. Lower branch of neutral stability curve for rotating-disk flow: (α,R)-plane using log-log scale.

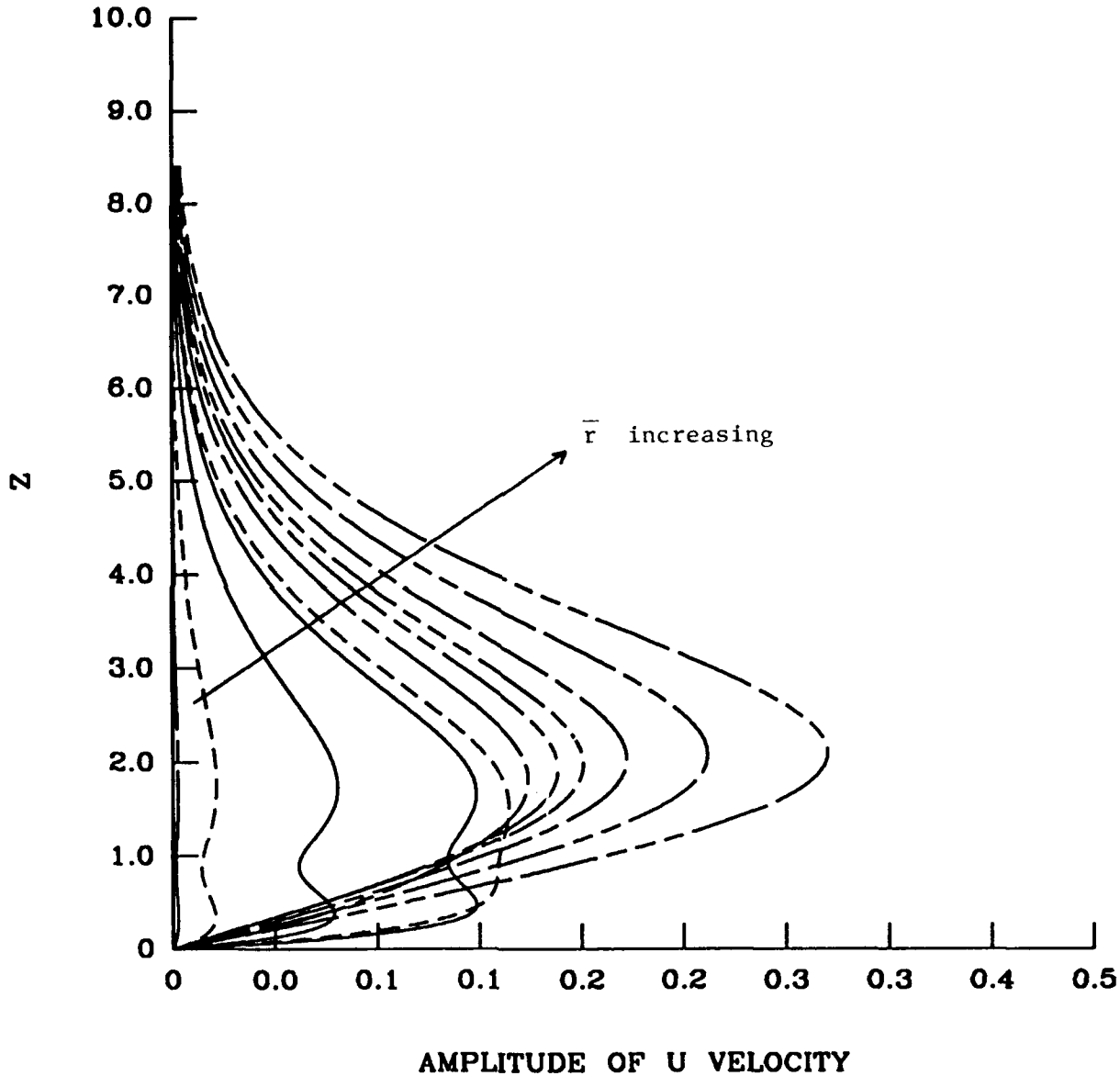

Fig. 3. Downstream development of velocity field for the case $\omega = 7.9$, $\beta = -.7$, $\sigma = 40$ at different $\bar{r} = .7, .8, .9, 1.0, 1.1, 1.25, 1.3, 1.4, 1.6$ and 1.9.

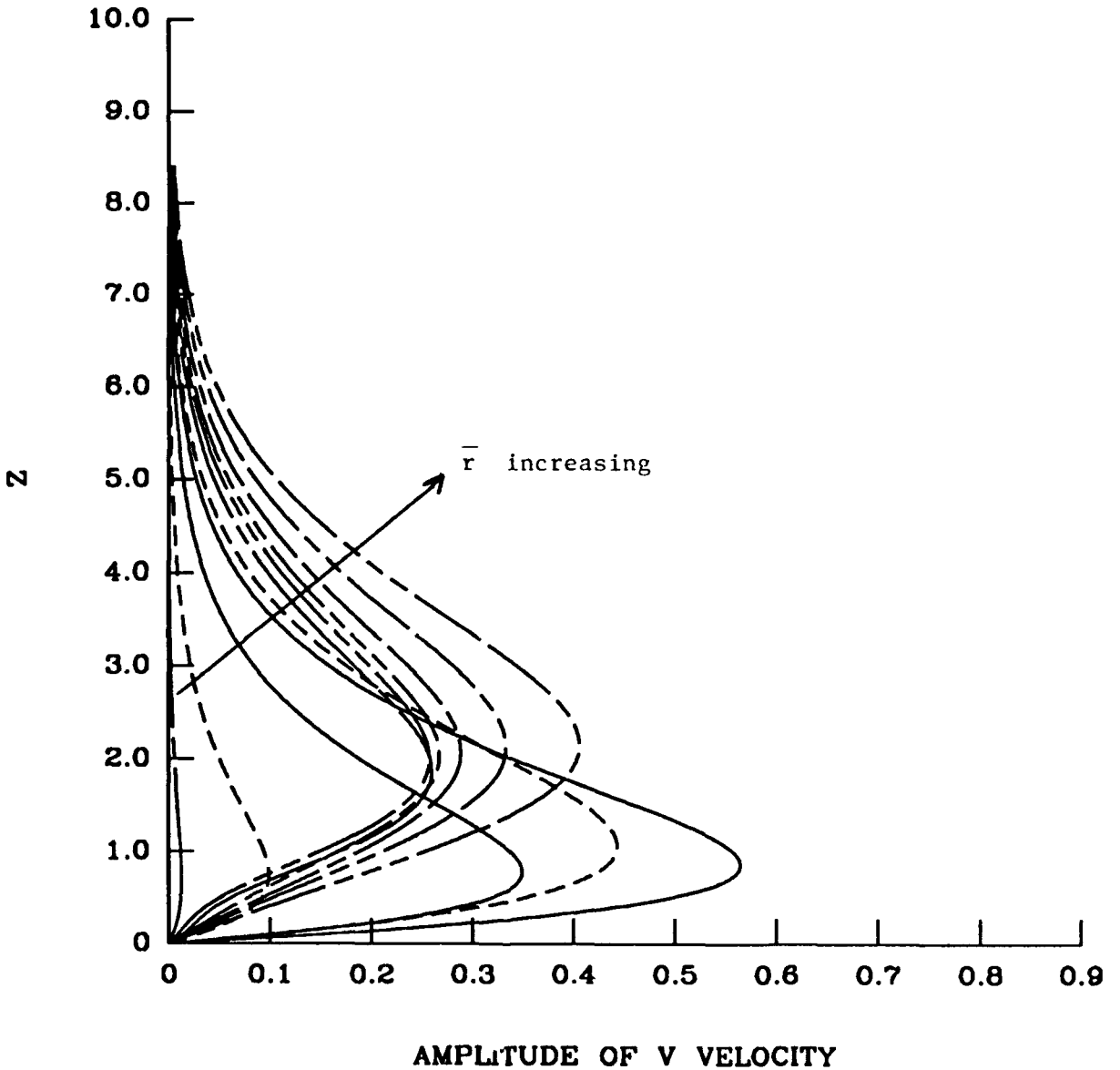

Fig. 4. Downstream development of velocity field for the case $\omega = 7.9$, $\beta = -7$, $\sigma = 40$ at different $\bar{r} = .7, .8, .9, 1.0, 1.1, 1.25, 1.3, 1.4, 1.6$ and 1.9.

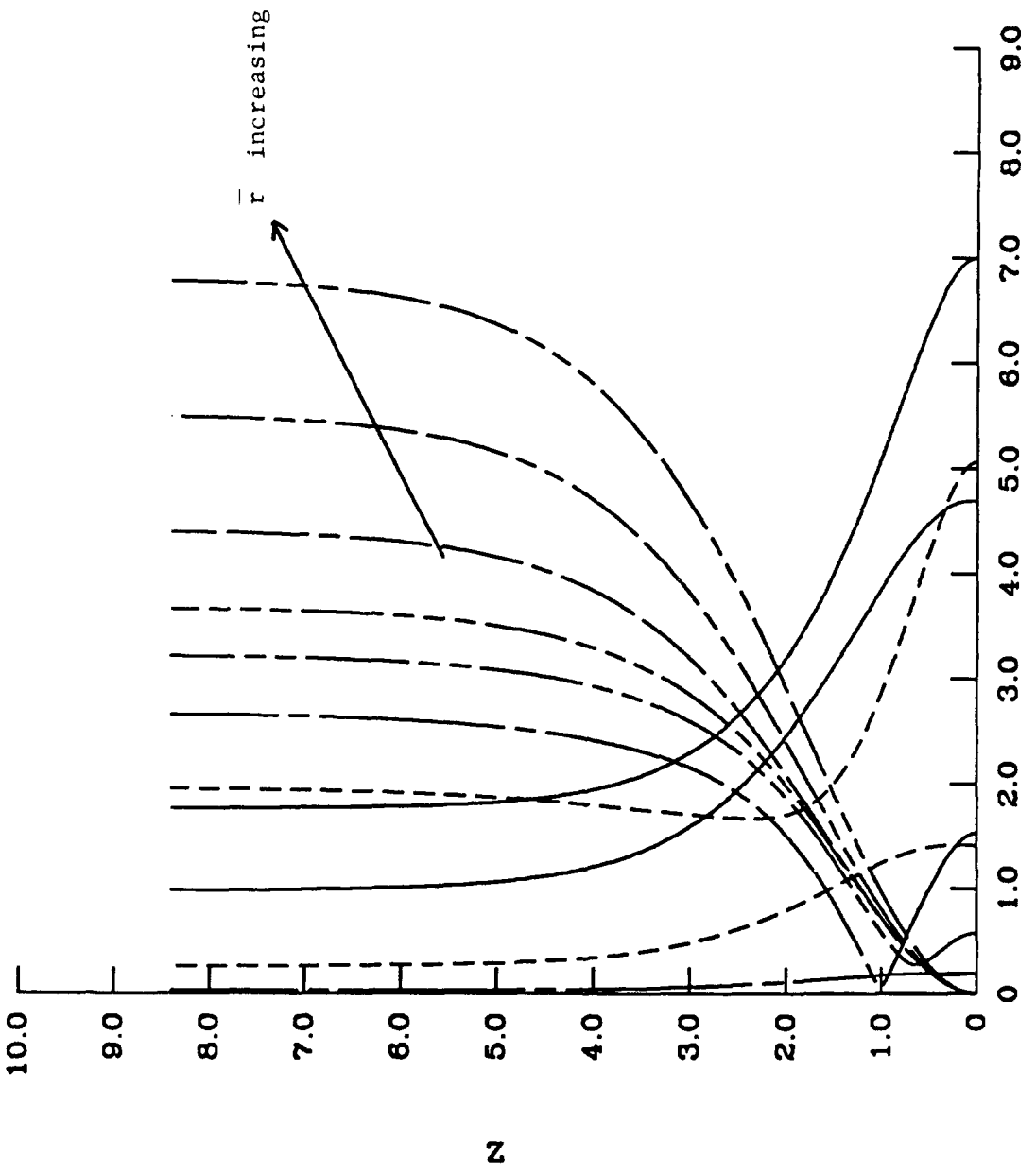

Fig. 5. Downstream development of velocity field for the case $\omega = 7.9$, $\beta = -7$, $\sigma = 40$ at different $\bar{r} = .7, .8, .9, 1.0, 1.1, 1.25, 1.3, 1.4, 1.6$ and 1.9.

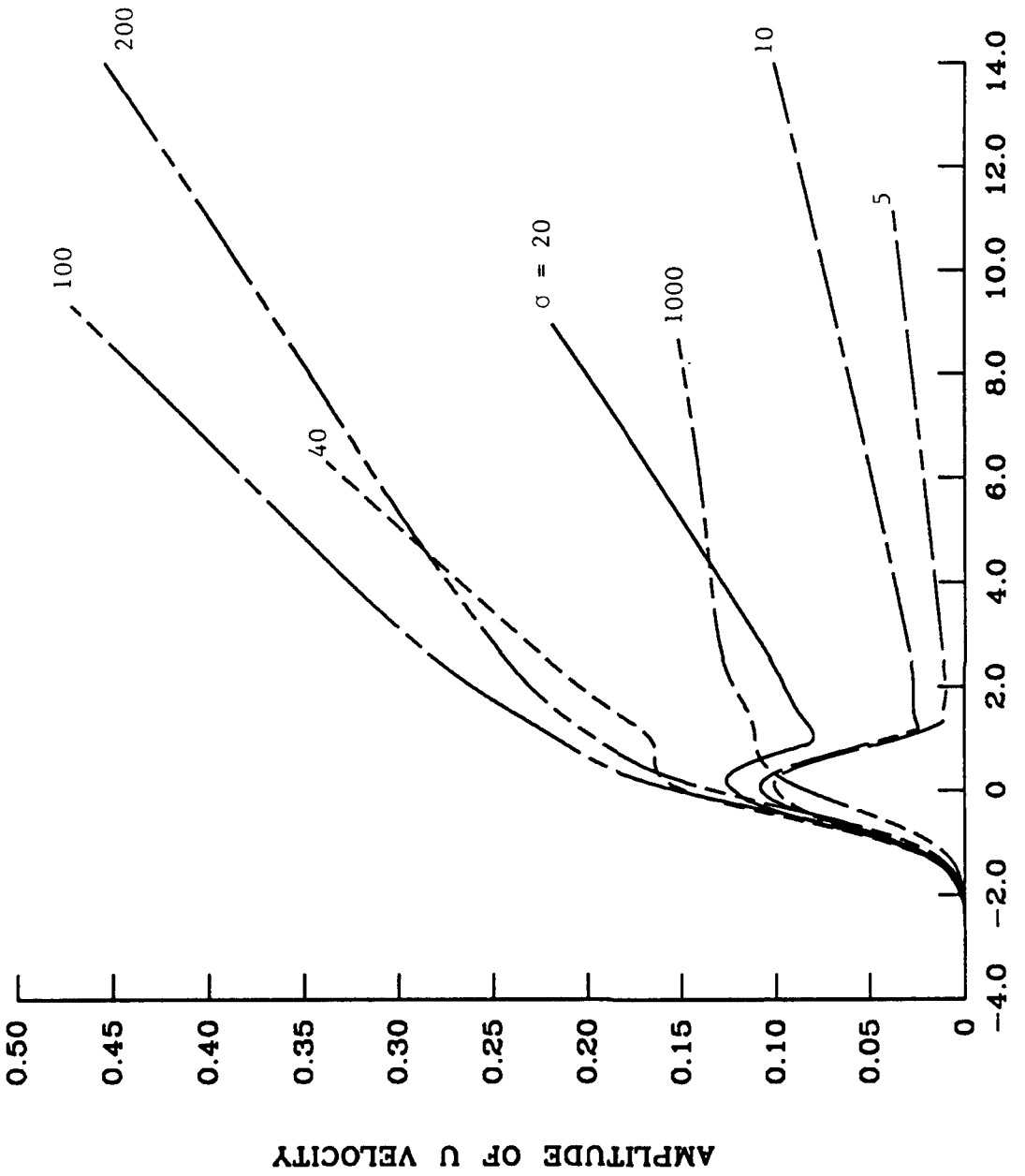

Fig. 6. Maximum amplitude of U_1 for the case $\omega = 7.9$, $\beta = -7$ at different σ.

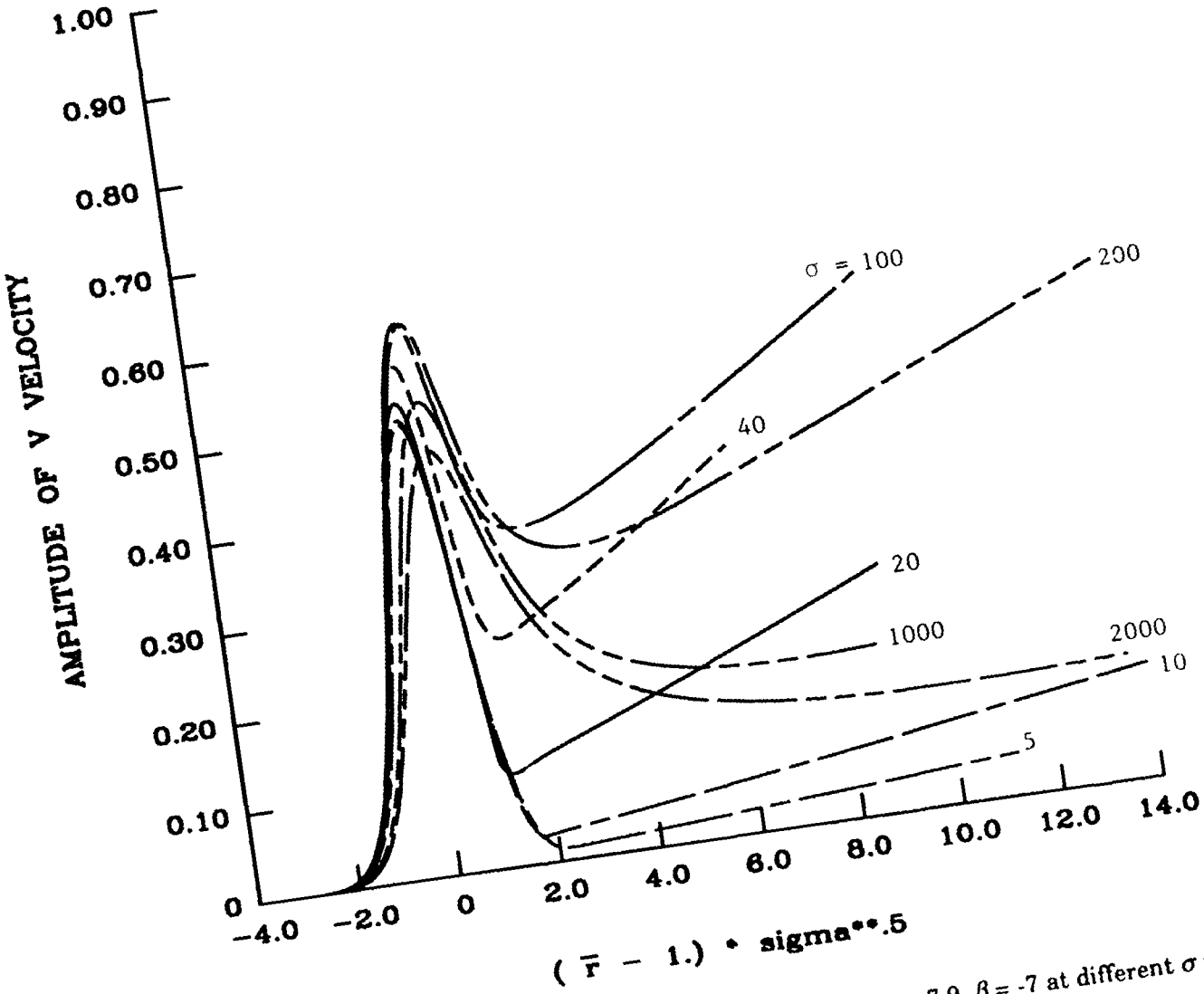

Fig. 7. Maximum amplitude of V_1 velocity for the case $\omega = 7.9$, $\beta = -7$ at different σ values.

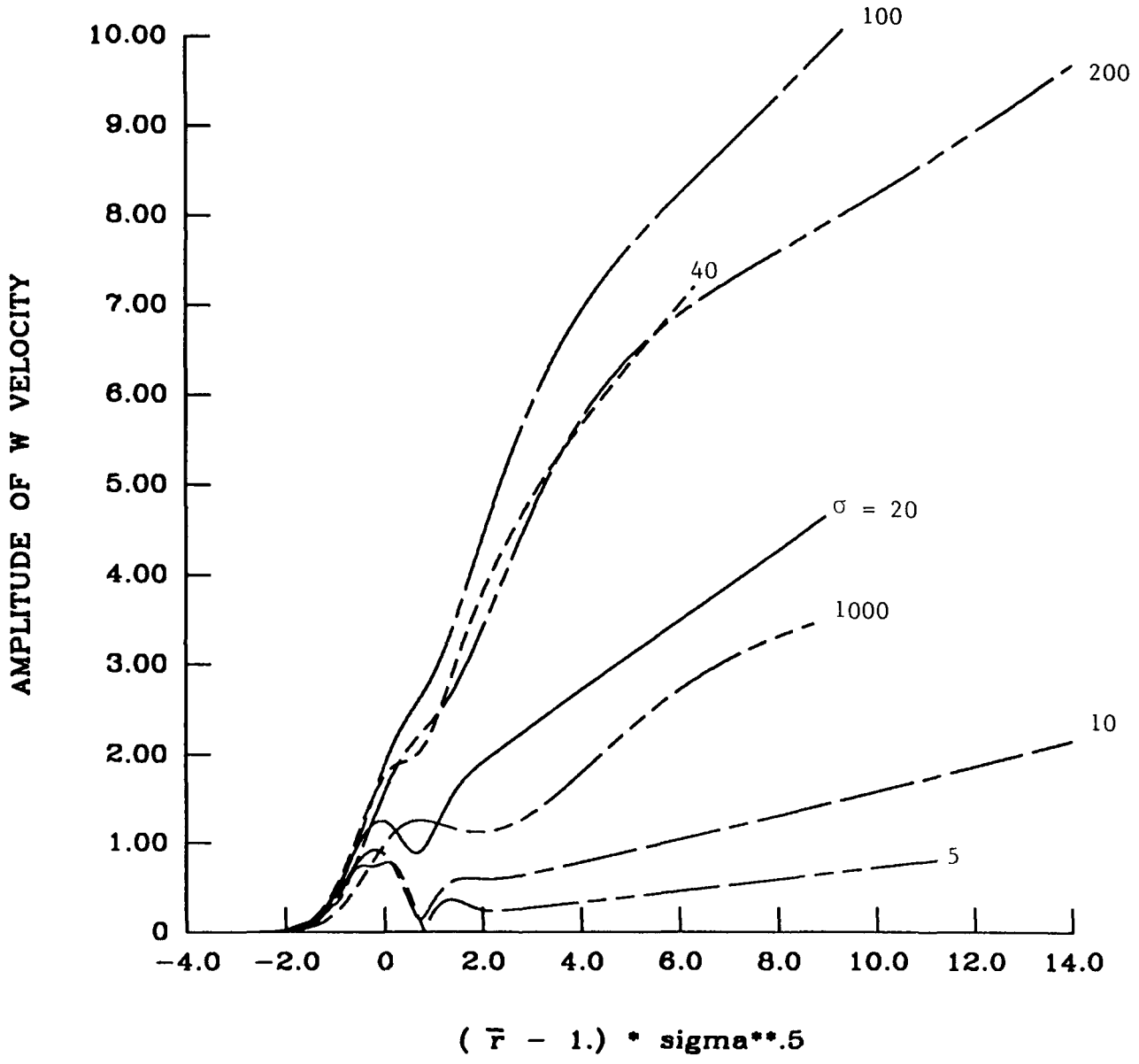

Fig. 8. Maximum amplitude of W_1 velocity for the case $\omega = 7.9$, $\beta = -7$ at different σ values.

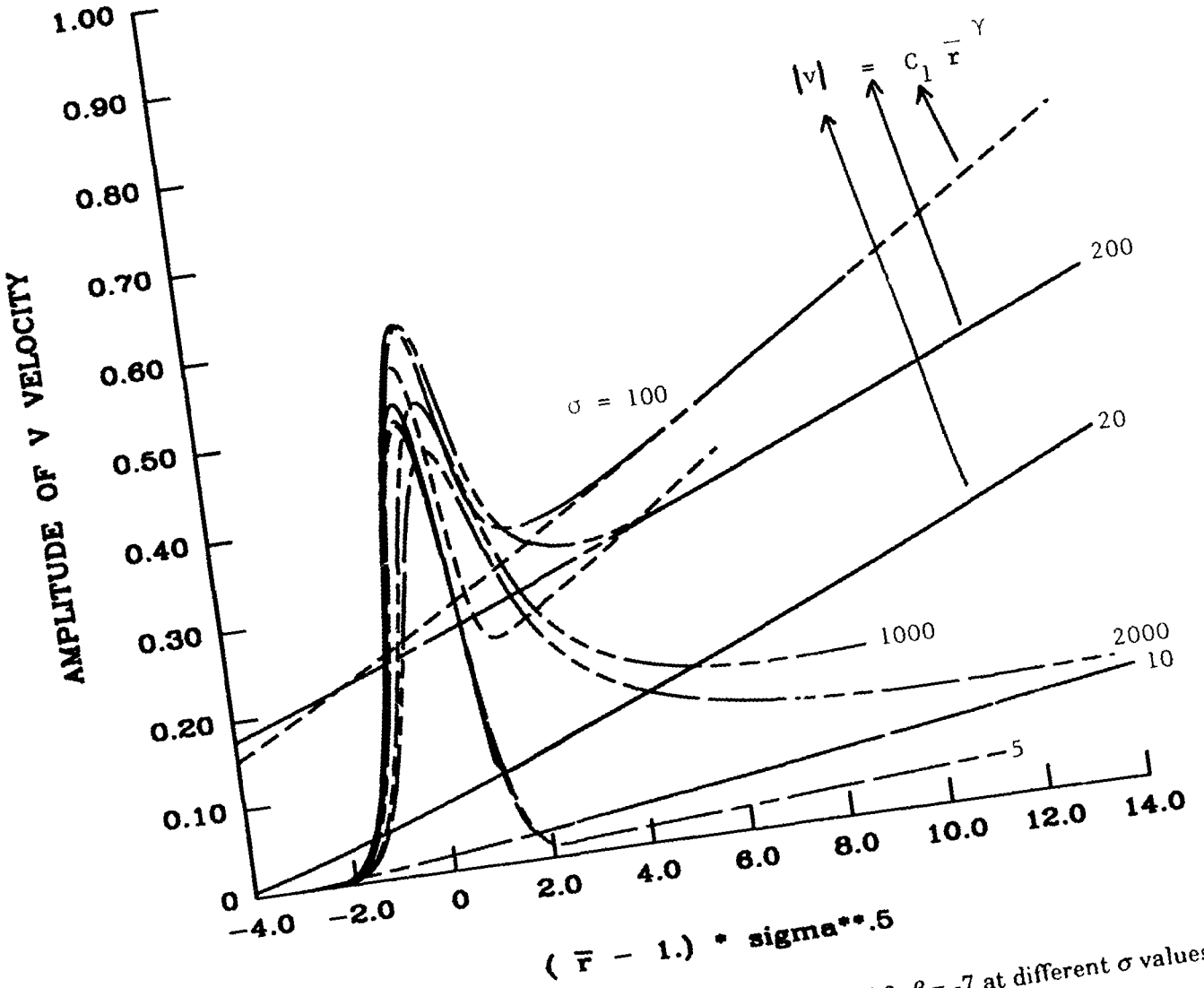

Fig. 9. Maximum amplitude of V_1 velocity for the case $\omega = 7.9$, $\beta = -.7$ at different σ values. $|V_1| = c_1 \bar{r}^{\gamma}$ is also drawn.

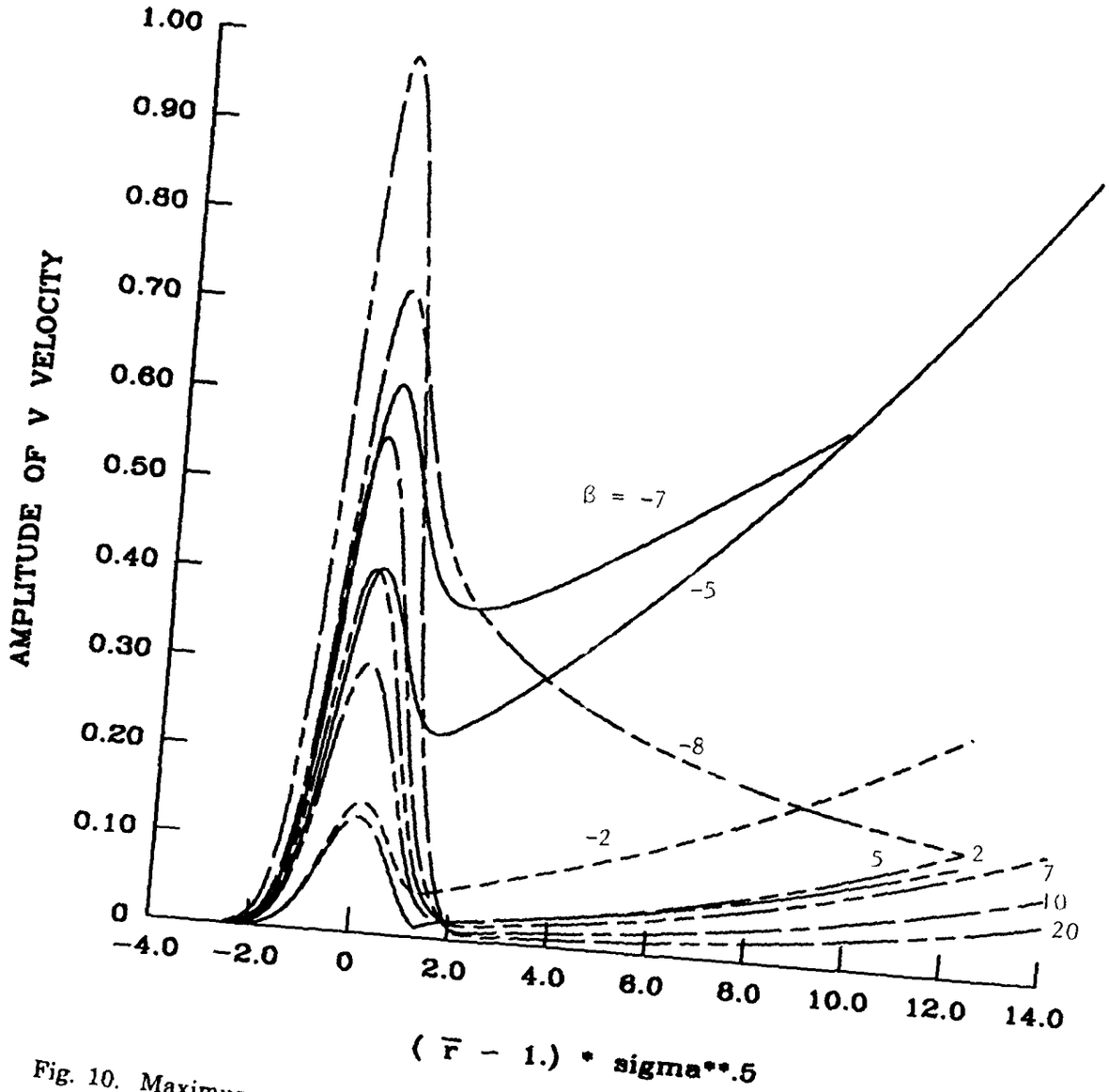

Fig. 10. Maximum amplitude of V_1 velocity for the case $\omega = 7.9$, $\sigma = 100$ at different β values.

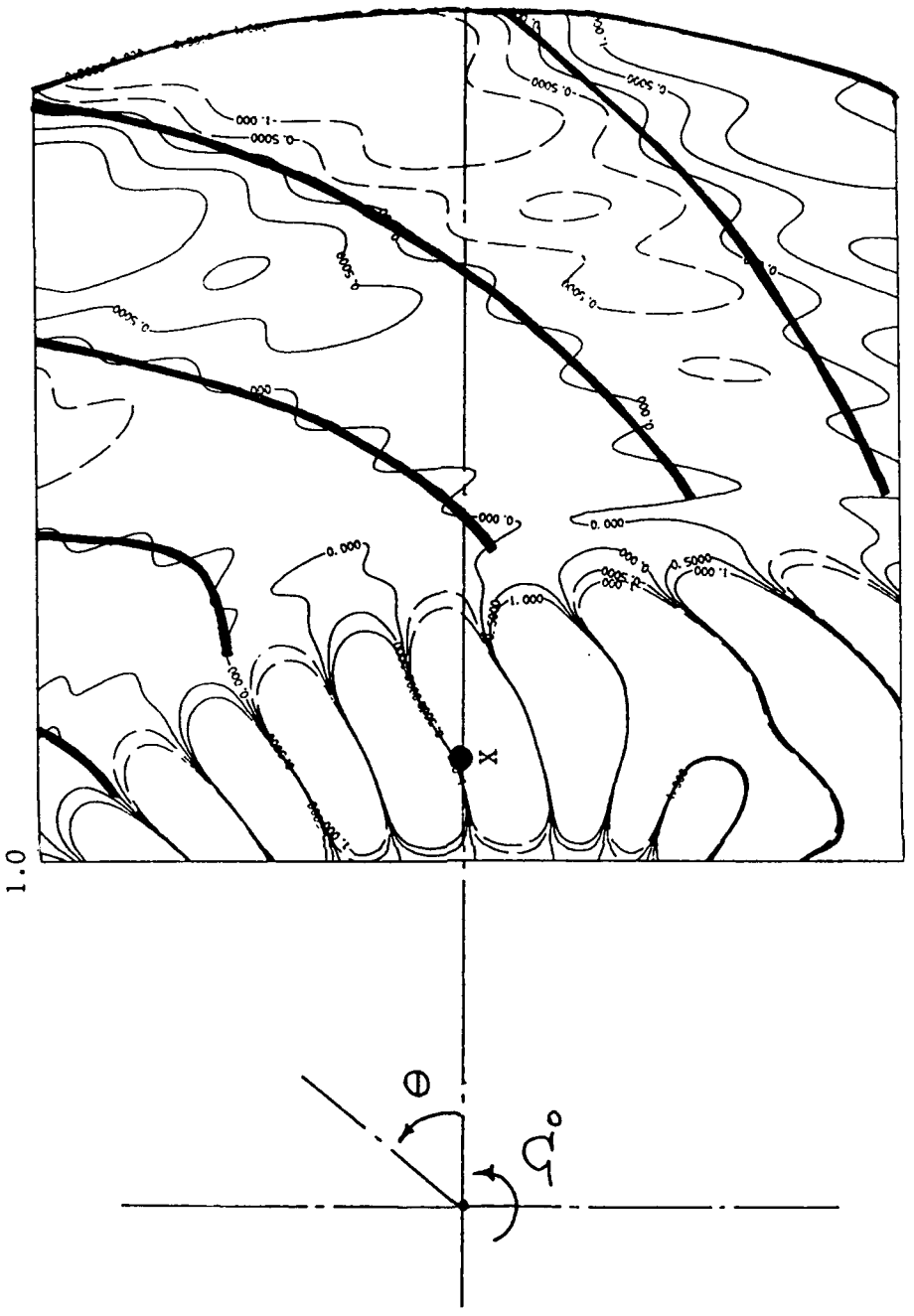

Fig. 11. Contour plots of V_1 velocity in (r,θ) plane at $z = 1.5$. $\omega = 7.9, \sigma = 100, a = b = .05$,

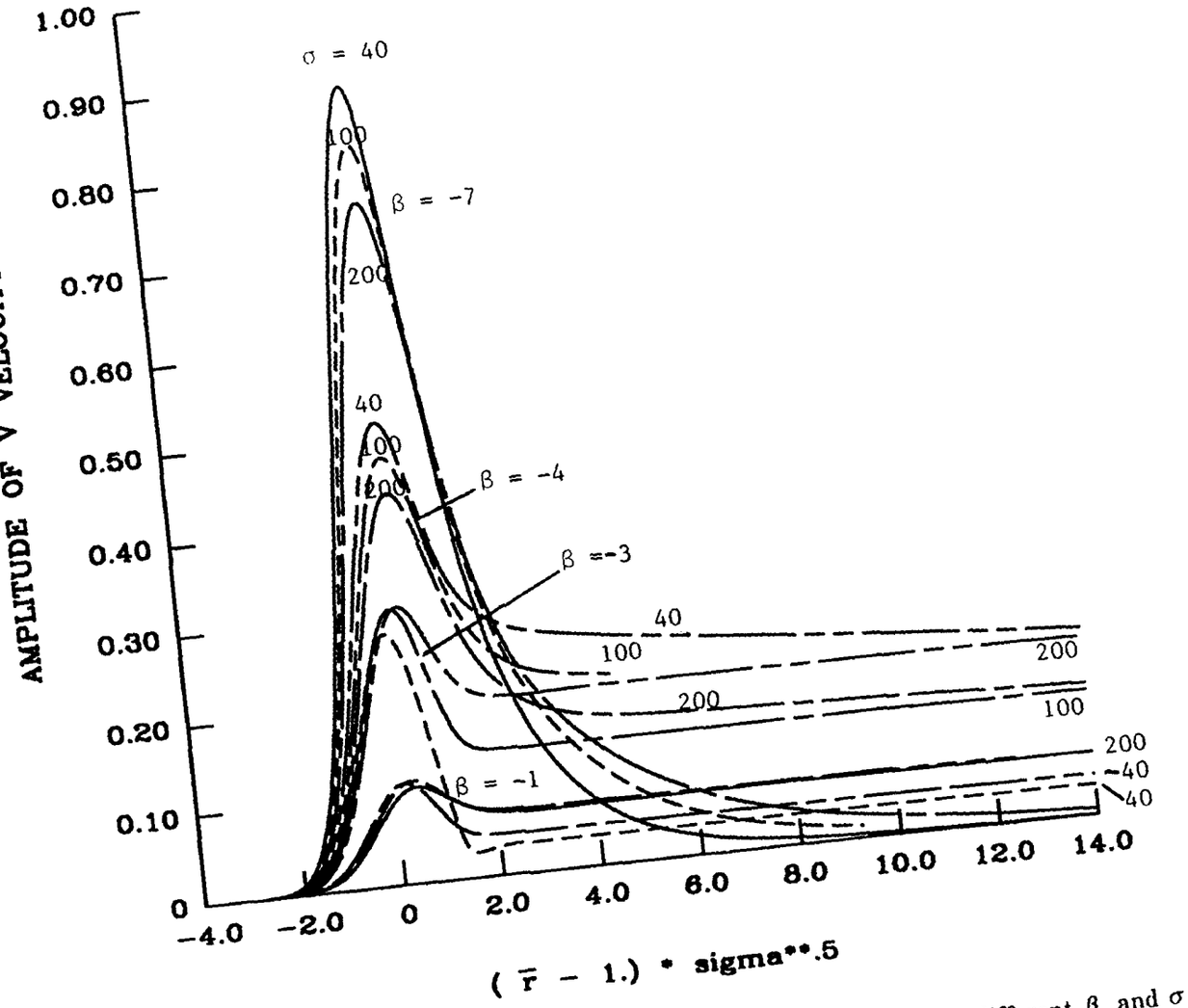

Fig. 12. Maximum amplitude of V_1 velocity for the case $\omega = 4.6$ at different β and σ values.

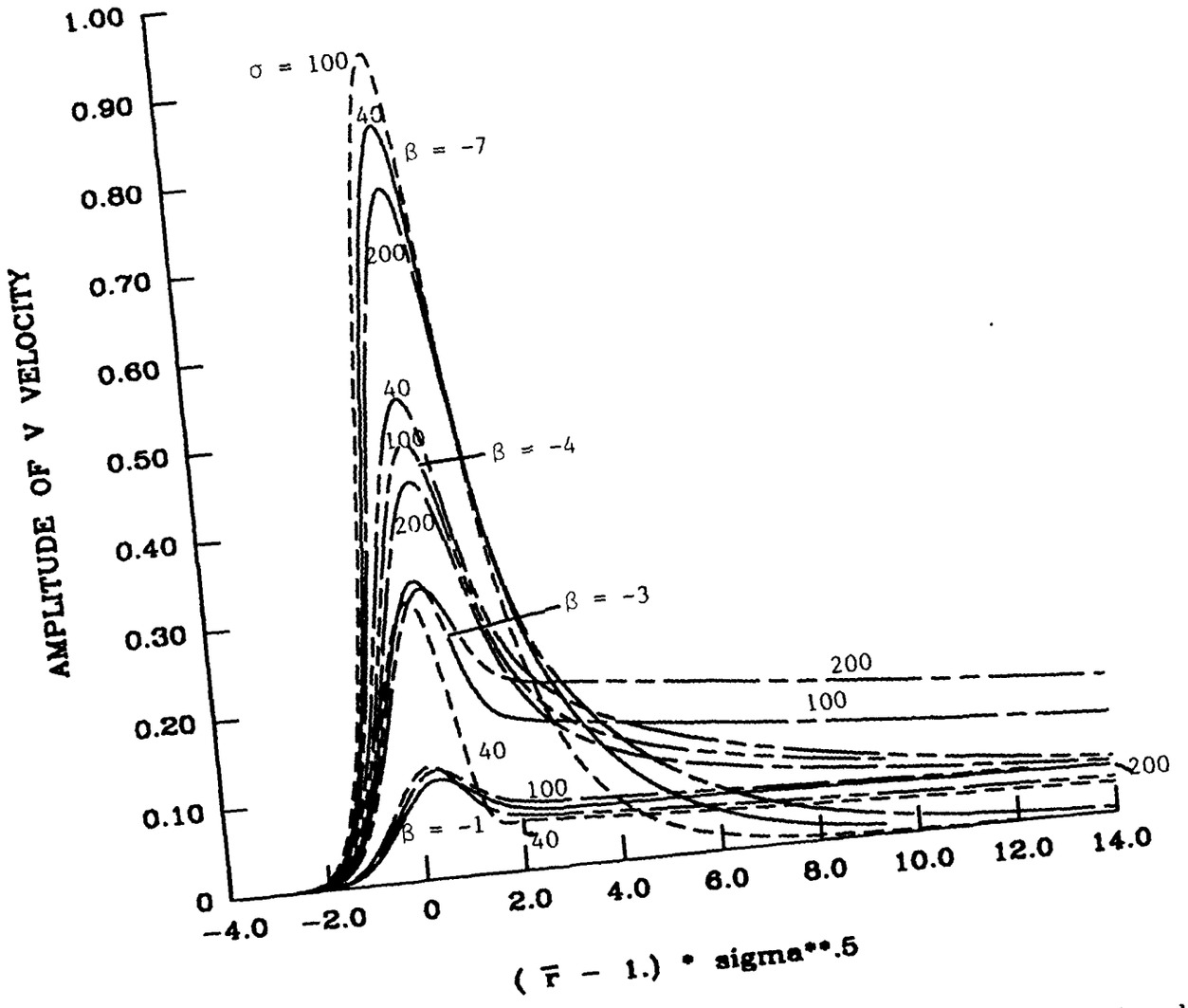

Fig. 13. Maximum amplitude of V_1 velocity for the case $\omega = 4.0$ at different β and σ values.

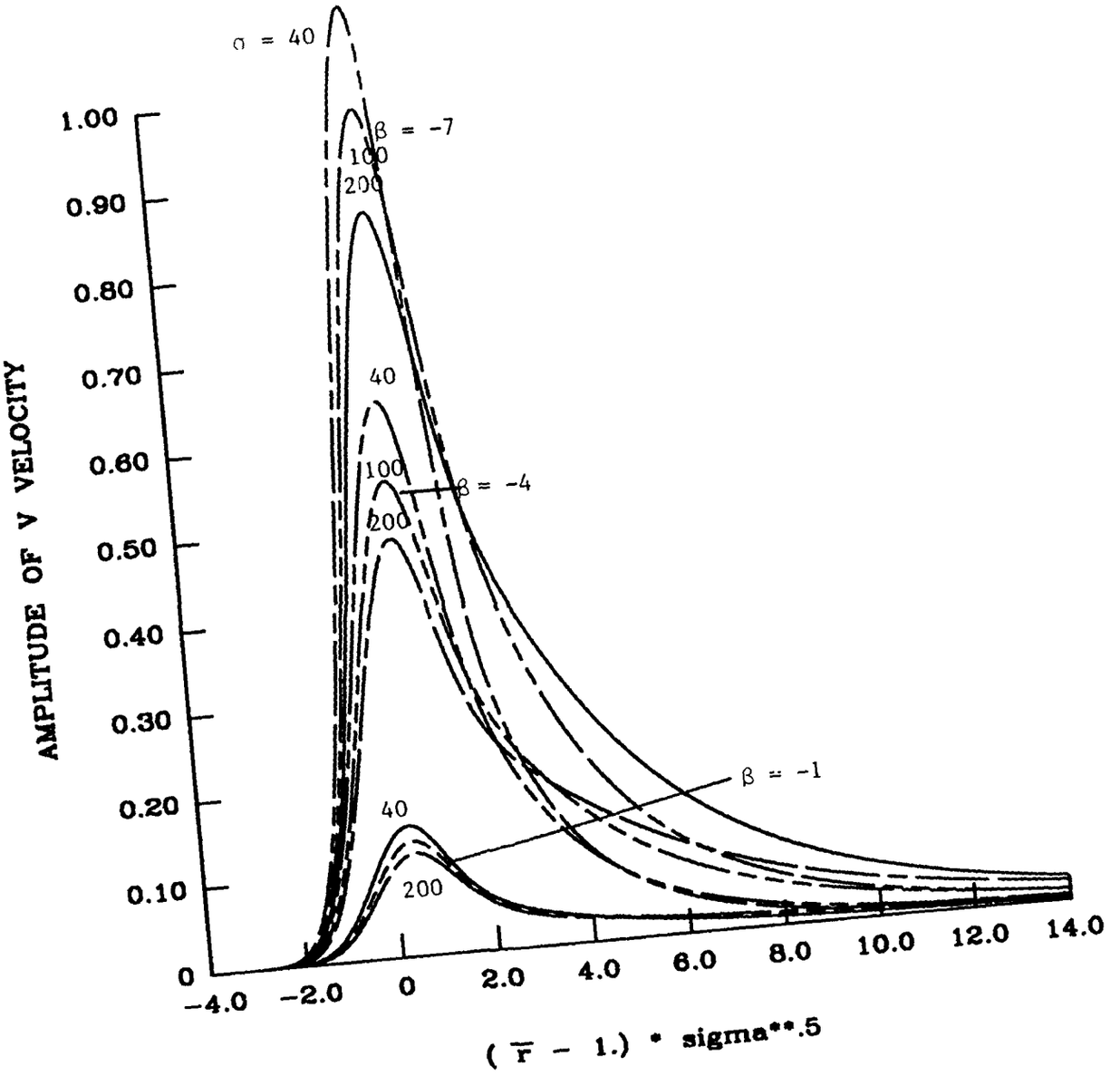

Fig. 14. Maximum amplitude of V_1 velocity for the case $\omega = 0.0$ at different β and σ values.

NASA National Aeronautics and Space Administration

Report Documentation Page

1. Report No.	2. Government Accession No.	3. Recipient's Catalog No.
NASA CR-187486 ICASE Report No. 90-89		

4. Title and Subtitle

ON THE RECEPTIVITY AND NON-PARALLEL STABILITY OF TRAVELLING DISTURBANCES IN ROTATING DISK FLOW

5. Report Date

December 1990

6. Performing Organization Code

7. Author(s)

P. Balakumar
P. Hall
M. R. Malik

8. Performing Organization Report No.

90-89

10. Work Unit No.

505-90-21-01

9. Performing Organization Name and Address

Institute for Computer Applications in Science and Engineering
Mail Stop 132C, NASA Langley Research Center
Hampton, VA 23665-5225

11. Contract or Grant No.

NAS1-18605

13. Type of Report and Period Covered

Contractor Report

12. Sponsoring Agency Name and Address

National Aeronautics and Space Administration
Langley Research Center
Hampton, VA 23665-5225

14. Sponsoring Agency Code

15. Supplementary Notes

Langley Technical Monitor:
Richard W. Barnwell

Submitted to Theoretical and Computational Fluid Dynamics

Final Report

16. Abstract

The generation and evolution of small amplitude long wavelength travelling disturbances in rotating disk flow is the subject of this paper. The steady rotational speed of the disk is perturbed so as to introduce high frequency oscillations in the flow field. Secondly, we introduce surface imperfections on the disk such as roughness elements. The interaction of these two disturbances will generate the instability waves whose evolution is governed by parabolic partial differential equations which are solved numerically. It is found that, for the class of disturbances considered here (wavelength on the order of Reynolds number), eigensolutions exist which decay or grow algebraically in the radial direction. However, these solutions grow only for frequencies larger than 4.58 times the steady rotational speed of the disk. The computed receptivity coefficient shows that there is an optimum size of roughness for which these modes are excited the most. The width of these roughness elements in the radial direction is about $.1r_0^*$ where r_0^* is the radial location of the roughness. It is also found that the receptivity coefficient is larger for a negative spanwise wavenumber than for a positive one. Typical wave angles for these disturbances are about -26^o.

17. Key Words (Suggested by Author(s))	18. Distribution Statement
disc, receptivity, stability	02 - Aerodynamics 34 - Fluid Mechanics and Heat Transfer Unclassified - Unlimited

19. Security Classif. (of this report)	20. Security Classif. (of this page)	21. No. of pages	22. Price
Unclassified	Unclassified	31	A03

NASA FORM 1626 OCT 86